Chapter 4
2D Materials: Molybdenum Disulfide for Electronic and Optoelectronic Devices

Shanee Pacley

4.1 Introduction

Two-dimensional (2D) materials such as graphene, molybdenum disulfide (MoS_2), tungsten diselenide (WSe_2), black phosphorus, and boron nitride (BN) have attracted much attention due to their extraordinary electronic and optical properties, making them ideal candidates for next-generation electronic and optoelectronic devices [1–4]. In particular, a monolayer of MoS_2 has a direct bandgap of 1.8–1.9 eV [5, 6], making it an ideal candidate for the mentioned applications [1, 2]. Growth processes of 2D MoS_2 include mechanical exfoliation [7–9], chemical vapor deposition (CVD) [5, 6], intercalation-assisted exfoliation [10–13], physical vapor deposition [14, 15], metal organic chemical vapor deposition [16], and a wet chemistry approach involving thermal decomposition of a precursor containing Mo and S [17]. An advantage of CVD growth of MoS_2 is the ability to grow large area films for device fabrication. Molybdenum disulfide films grown using CVD have demonstrated promising results for semiconductor grade material properties, with observed field-effect mobilities around 500 cm^2/Vs [18]. During CVD growth, sulfurization of molybdenum-containing precursors such as Mo, MoO_3, and $MoCl_5$ is usually performed. In the case of MoO_3 [6] and $MoCl_5$ [19], the precursors have been powders or ribbons, whereas Mo has been prepared by e-beam evaporation [5] or sputtering [20]. At the Air Force Research Laboratory, we observed the structure properties of MoS_2 films grown by sulfurization of DC magnetron sputtered MoO_3 and Mo precursor films at room temperature. In addition, reduced graphene oxide (rGO), known for increasing layer and domain size of MoS_2 [21, 22], was incorporated in our growth process of MoS_2. This chapter will be focused on our reported data related to this work.

S. Pacley (✉)
Materials and Manufacturing Directorate, Air Force Research Laboratory,
Wright-Patterson Air Force Base, OH, USA
e-mail: shanee.pacley@us.af.mil

© Springer Nature Switzerland AG 2020

M. E. Kinsella (ed.), *Women in Aerospace Materials*, Women in Engineering and Science, https://doi.org/10.1007/978-3-030-40779-7_4

4.2 MoS_2 Research

Thin films of metallic Mo and MoO_3 were sputtered on c-face sapphire substrates (diameter of 25.4 mm) using a DC magnetron sputtering system (500 V at 100 mA) at room temperature, with an argon pressure of 0.92 Pa. The thickness of the precursor (3 nm for both Mo and MoO_3) was controlled by manipulating the sputtering so that there were equal amounts of Mo sputtered in the MoO_3 and Mo films. Table 4.1 lists the precursors and sample names. The substrates were ultrasonically cleaned in acetone for 5 minutes prior to deposition of Mo and MoO_3. Following sputtering of Mo and MoO_3 onto the substrates, the precursors were separately placed in the center of the quartz tube (Fig. 4.1). Sulfur powder (2 g) was placed in a ceramic boat, upstream from the Mo and MoO_3 films. Reduced graphene oxide (Sigma-Aldrich) was dispersed in isopropyl alcohol and drop cast on separate sapphire substrates. The rGO samples were air dried before they were placed in the furnace next to the sputtered precursor films of Mo and MoO_3 (with a distance of 5 mm between the precursor and rGO samples). After pumping the furnace down to a vacuum pressure of 667 Pa, the samples were heated to 300 °C at 20 °C/min and held there for 15 minutes. This enabled the removal of any residual water molecules. Next, the

Table 4.1 List of thicknesses used for Mo and MoO_3 precursor films

Sample (*r*-rGO)	Precursor	Precursor thickness
S1, S1*r*	Mo	3 nm
S2, S2*r*	MoO_3	3 nm

Reproduced from Pacley et al. [3], with the permission of the American Vacuum Society
r indicates rGO was used during experiments

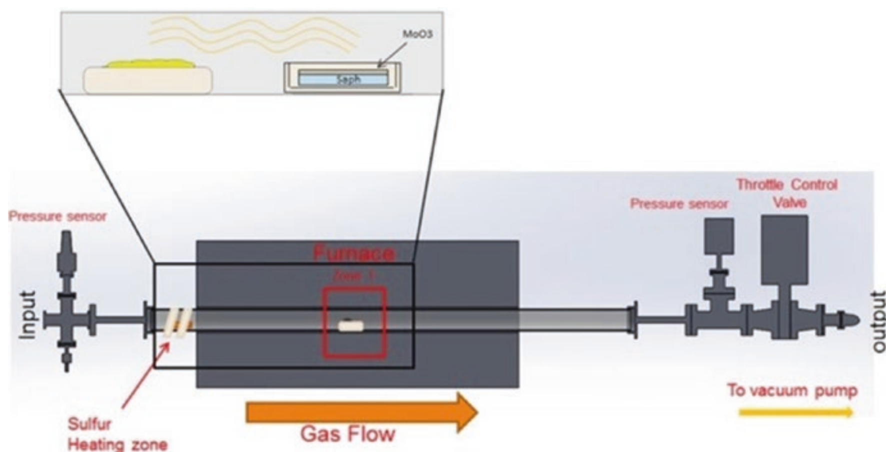

Fig. 4.1 Chemical vapor deposition setup for MoS_2 growth on Al_2O_3 substrates. (Reproduced from Pacley et al. [3], with the permission of the American Vacuum Society)

precursors were heated to 850 °C at a rate of 20 °C/min. As the temperature of the furnace approached 850 °C (around 830 °C), the boat with sulfur was heated to 125 °C using a heating tape. Both the precursors and the sulfur were held at their temperatures for 1 hour, followed by cooling to room temperature. All experiments were performed in an Ar/H_2 environment, with a flow rate of 75 sccm.

Transmission electron microscopy (TEM) imaging of the MoS_2 film cross sections for samples S1 (MoS_2 grown from Mo precursor) and S1*r* (MoS_2 film grown using Mo precursor with rGO seed) are shown in Fig. 4.2 [3]. The precursor films, MoO_3 and Mo, are both shown in Fig. 4.2a, b [3]. Samples S1 and S1*r* (Fig. 4.2c, e) show uniform and continuous layer growth of MoS_2 [3]. Both samples have a thickness of 7–8 nm, indicating the rGO used during the CVD growth of sample S1*r* had no effect on the film thickness. Atomic force microscopy (AFM) showed that samples S1 and S1*r* had an RMS of 0.360 nm and 2.43 nm (respectively), and the grain size increased from 4.5 nm to 17.7 nm, respectively (see Fig. 4.3a, b) [3]. This increase in the grain size indicated that the rGO played a role in grain growth of the MoS_2. In contrast to the uniform and continuous film growth of samples S1 and S1*r*, samples S2 (MoO_3 precursor) and S2*r* (MoO_3 precursor with rGO seed) demonstrated a non-uniform, outward growth of MoS_2 (Fig. 4.2d, f) [3]. It is reported that at 600 °C, MoO_3 reduces to MoO_2 under an H_2 environment [23]. In this research, there was indication that MoO_2 had formed after annealing MoO_3 at 850 °C. X-ray photoelectron spectra (Fig. 4.4a) showed peaks at 229.57 and 232.7 for Mo(IV), which is typical of MoS_2 and MoO_2, and 232.19 and 235.32 for Mo(VI), which is typical of MoO_3. AFM was performed on the same annealed sample (Fig. 4.3c) [3], and we noticed small islands across the substrate. The islands were formed when the sputtered MoO_3 film reduced to MoO_2 during annealing at 850 °C. Consequently, sulfurization of MoO_2 islands caused MoS_2 growth in a Volmer-Weber growth mechanism, which is a result of the film not wetting the substrate [24]. Moser and Levy reported similar growth patterns using sputtering technique to deposit thick MoS_2 films [25].

Figure 4.3d, e shows the grain structures of MoS_2 grown using the sputtered MoO_3 films (S2 and S2*r*) [3]. The RMS values for these samples were 2.00 nm (S2) and 3.66 nm (S2*r*), and the grain size increased from 7.9 nm (S2) to 12.2 nm (S2*r*) when rGO was used during the growth. This correlates well with the data from samples S1 and S1*r* that suggest rGO promotes grain growth when using sputtered precursor films. There was also a decrease in the film thickness, going from 15 nm (S2) to 7 nm (S2*r*) when rGO was used during the sulfurization process (Fig. 4.2d, f). Ling et al. [22] report that organic seed promoters (such as PTAS) enable heterogeneous nucleation sites and that the size of the MoS_2 domains is dependent upon the distance of the seed promoter from the precursor. We believe this is what occurred when rGO was used in our experiments involving sputtered Mo and MoO_3 films. However, further investigation needs to be conducted to better understand the kinetics, and mechanism of increasing grain size, when using rGO during the sulfurization sputtered films.

X-ray photoelectron spectroscopy (XPS) was performed for composition and chemistry analysis of the films that were grown in this research. The survey spectra

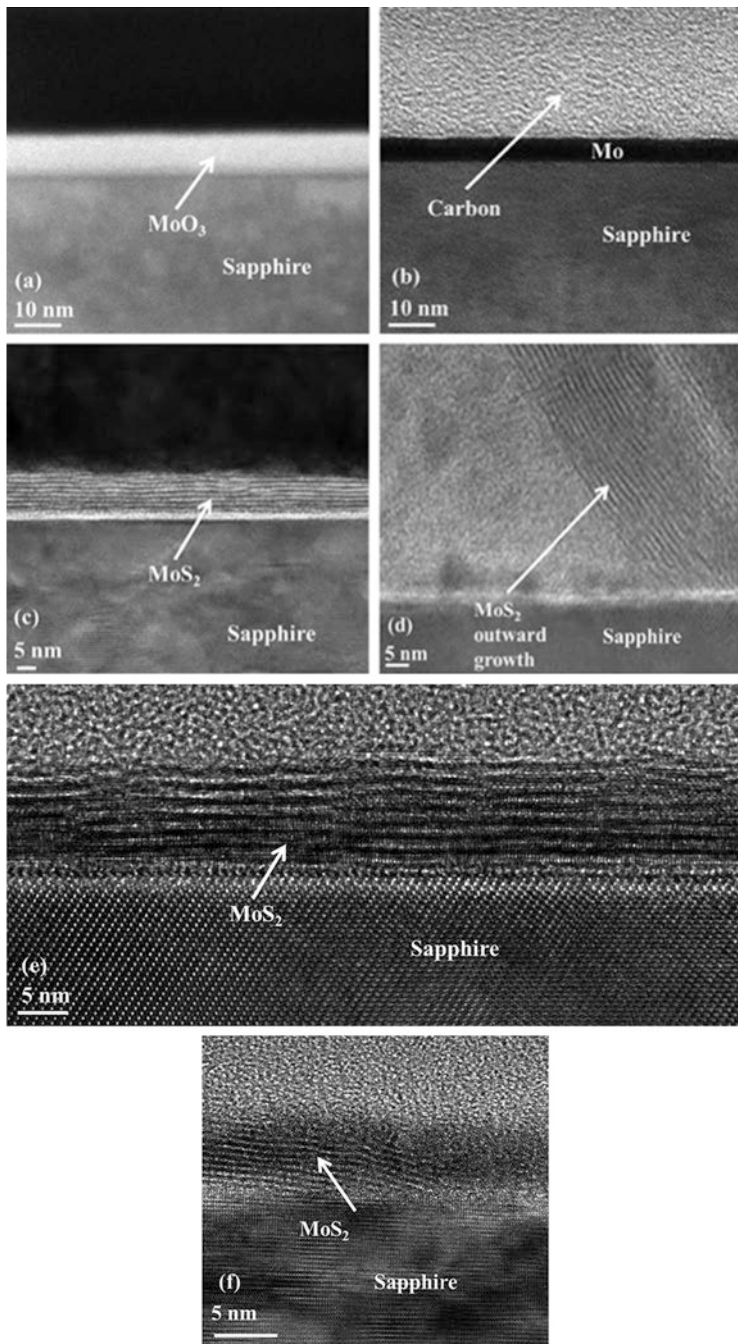

Fig. 4.2 TEM image of (**a**) MoO_3 precursor film used for MoS_2 growth; (**b**) Mo precursor film for MoS_2 growth; (**c**) sample S1 (MoS_2 on sapphire using Mo precursor) showing a layer thickness of 7 nm; (**d**) sample S2 (MoS_2 on sapphire using a MoO_3 precursor) showing an outward growth of MoS_2, with a thickness of 15 nm; (**e**) sample S1*r* (Mo precursor) using rGO with a measured thickness of 7–8 nm; and (**f**) sample S2r (MoO_3) using rGO with a thickness of 7 nm. (Reproduced from Pacley et al. [3], with the permission of the American Vacuum Society)

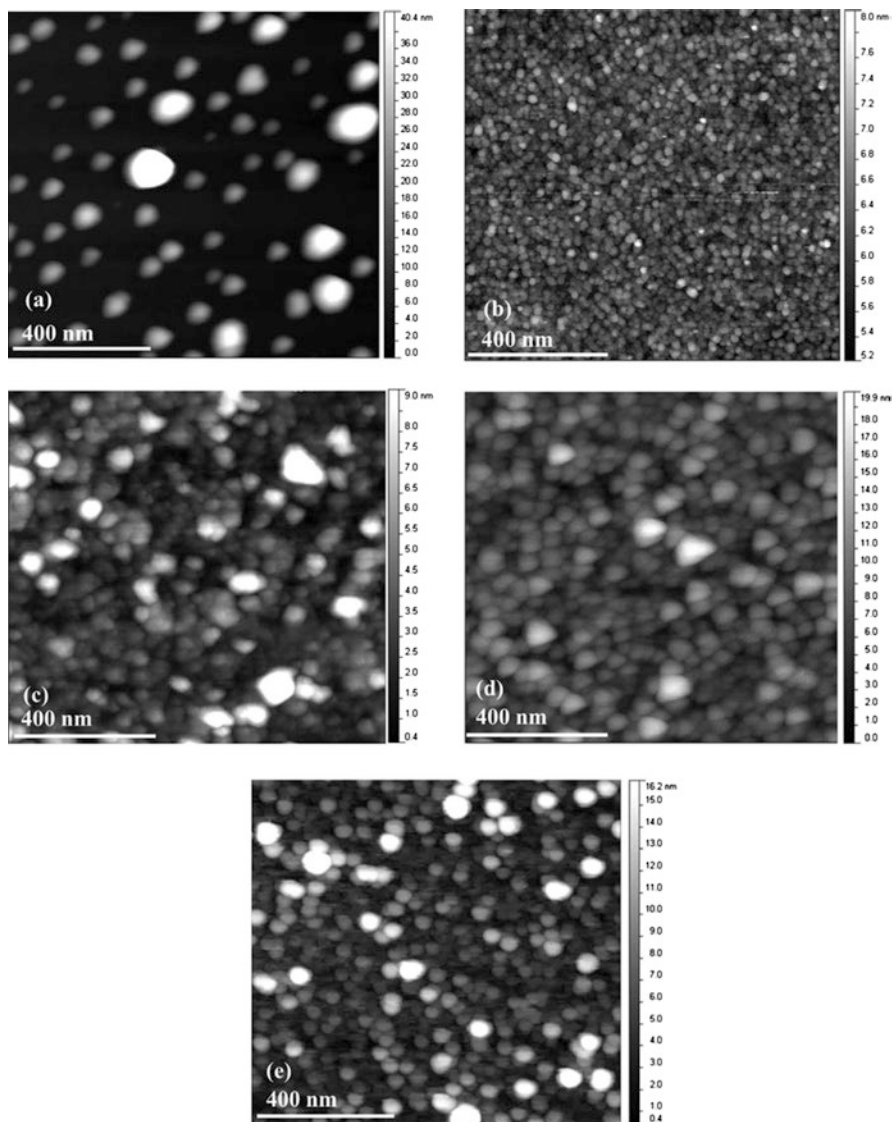

Fig. 4.3 AFM surface topography (1 × 1 μm) for (**a**) MoO3 precursor that was heated to 850 °C forming MoO_2 islands; (**b**) sample S1 (Mo precursor) showing a dense film of MoS_2 with a grain size of 4.4 nm; (**c**) MoS_2 sample S2 (MoO_3 precursor) with a grain size of 7.9 nm; (**d**) MoS_2 of MoS_2, with a thickness of 15 nm; (**e**) sample S1*r* (Mo precursor) using rGO with a measured thickness of 7–8 nm; and (**f**) sample S2r (MoO_3) using rGO with a thickness of 7 nm. (Reproduced from Pacley et al. [3], with the permission of the American Vacuum Society)

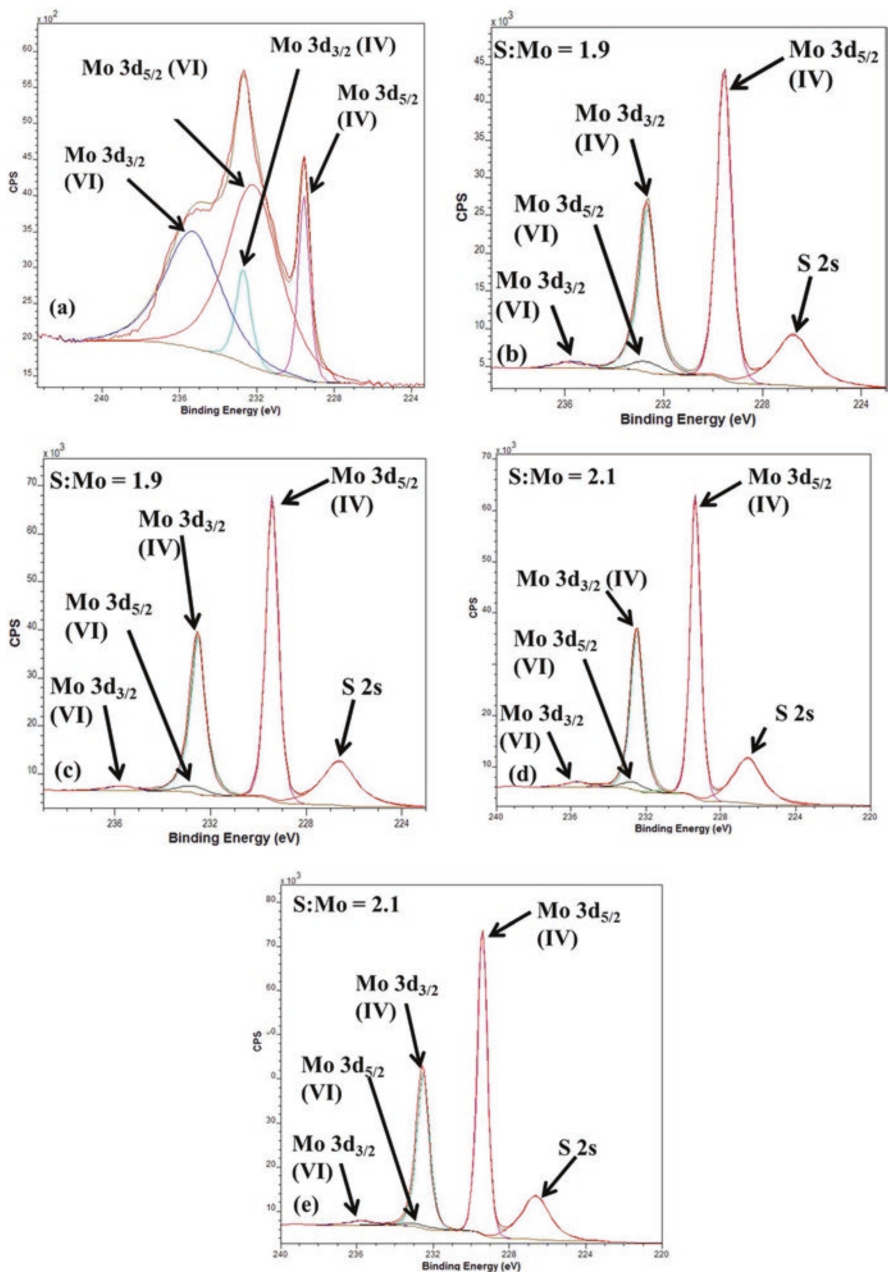

Fig. 4.4 XPS spectra of annealed MoO3, MoS_2 films S1(MoS_2 using Mo precursor), S2 (MoS_2 using MoO_3 precursor), S1*r* (MoS_2 using Mo precursor and rGO), and S2*r* (MoS_2 using MoO_3 precursor and rGO). The annealed MoO_3 (**a**) shows Mo(IV) peaks which are indicative of MoO_2 and Mo(VI) peaks that occur when MoO_3 is present. Both (**b**) and (**c**) show spectra for samples S1 and S2, respectively, having a stoichiometric structure. In (**d**) and (**e**), the stoichiometry has increased for samples S1*r* and S2*r*, respectively, indicating the rGO played a role in increasing the stoichiometry. (Reproduced from Pacley et al. [3], with the permission of the American Vacuum Society)

(not shown) from sulfurized thin films of samples S1/S1*r* and S2/S2*r* showed peaks from Mo and S, as expected. As mentioned previously, Fig. 4.4a shows the spectra for annealed MoO_3 [3]. The influence of the rGO on MoS_2 stoichiometry was analyzed by comparing the S:Mo ratios obtained from the XPS spectra. The MoS_2 films grown from samples S1 and S1*r* had S:Mo ratios of 1.9 and 2.1, respectively (see Fig. 4.4b, d). Samples S2 and S2*r* demonstrated the same respective S:Mo ratios of 1.9 and 2.1 (see Fig. 4.4c, e). The apparent improvement in the film stoichiometry is most likely a result of the Mo:S averaging over large spot size analysis area in XPS, which is orders of magnitude larger when compared to the average grain sizes of synthesized MoS_2 films. The presence of the rGO helped to increase the MoS_2 grain size areas and correspondingly decrease contributions of photoelectrons escaped from the grain boundary areas.

Curve fits to the Mo 3d doublets for all of the samples revealed two populations of Mo atoms. The Mo $3d_{5/2}$ peak at 229.8 eV and Mo $3d_{3/2}$ peak at 232.9 eV reveal the presence of Mo(IV), with a binding energy typical of MoS_2 or MoO_2 [26]. The Mo $3d_{5/2}$ peak at 232.7 eV and Mo $3d_{3/2}$ peak at 235.8 eV indicate the presence of Mo(VI), with a binding energy typical of MoO_3 [27]. This suggests that there is likely some MoO_2 present at the surface or at grain boundaries within the films. However, the intensity for both the Mo(IV) and Mo(VI) peaks are so low, that the presence of MoO_2 and MoO_3 is negligible.

4.3 Conclusion

The influence of metallic Mo and MoO_3 thin-film precursors on the structure of MoS_2 films grown by CVD was investigated. TEM established that rGO did not have an impact on the MoS_2 film thickness for sputtered Mo but that it was responsible for the increase in the grain size. We also observed an increase in the grain size when rGO was used during sulfurization of sputtered MoO_3. Reports demonstrate that seed promoters diffuse onto growth substrates, acting as nucleation sites for MoS_2 growth. In addition, the size of the MoS_2 domains is dependent upon the distance between the seed promoter and the growth substrate. In conclusion, sputtered Mo precursor films produce better uniformity and continuous MoS_2 films, making these nanocrystalline films potentially applicable for electronic and optoelectronic devices.

References

1. B. Radisavljevic, A. Radenovic, J. Brivio, et al., Single-layer MoS_2 transistors. Nat. Nanotechnol. **6**, 147 (2011)
2. Z. Yin, H. Li, H. Li, et al., Single-layer MoS_2 phototransistors. ACS Nano **6**(1), 74 (2012)

3. S. Pacley, J. Hu, M. Jespersen, et al., Impact of reduced graphene oxide on MoS_2 grown by sulfurization of sputtered MoO_3 and Mo precursor films. J. Vac. Sci. Technol. A **34**(4), 041505–041501 (2016)
4. D.Y. Zemlyanov, M. Jespersen, D.N. Zakharov, et al., Versatile technique for assessing thickness of 2D layered materials by XPS. Nanotechnology **29**(115705), 1 (2018)
5. Y. Zhan, Z. Liu, S. Najmaei, et al., Large-area vapor-phase growth and characterization of MoS_2 atomic layers on a SiO_2 substrate. Small **8**(7), 966 (2012)
6. S. Najmaei, Z. Liu, X. Zou, et al., Vapour phase growth and grain boundary structure of molybdenum disulphide atomic layers. Nat. Mater. **12**(8), 754 (2013)
7. B. Radisavljevic, M.B. Whitwick, A. Kis, Integrated circuits and logic operations based on single-layer MoS_2. ACS Nano **5**(12), 9934 (2011)
8. K.F. Mak, C. Lee, J. Hone, et al., Atomically thin MoS_2: A new direct-gap semiconductor. Phys. Rev. Lett. **105**, 136805–136801 (2010)
9. J. Brivio, D.T.L. Alexander, A. Kis, Ripples and layers in ultrathin MoS_2 membranes. Nano Lett. **11**(12), 5148 (2011)
10. H. Ramakrishna Matte, A. Gomathi, A. Manna, et al., MoS_2 and WS2 analogues of graphene. Angew. Chem. Int. Ed. **49**(24), 4059–4062 (2010). https://doi.org/10.1002/anie.201000009
11. Z. Zeng, Z. Yin, X. Huang, et al., Single-layer semiconducting nanosheets: High-yield preparation and device fabrication. Angew. Chem. Int. Ed. **50**(47), 11093–11097 (2011). https://doi.org/10.1002/anie.201106004
12. V. Nicolosi, M. Chhowalla, M.G. Kanatzidis, et al., Liquid exfoliation of layered materials. Science **340**(6139), 1226419 (2013). https://doi.org/10.1126/science.1226419
13. G. Eda, H. Yamaguchi, D. Voiry, et al., Photoluminescence from chemically exfoliated MoS_2. Nano Lett. **11**(12), 5111–5116 (2011). https://doi.org/10.1021/nl201874w
14. C. Muratore, A.A. Voevodin, Control of molybdenum disulfide basal plane orientation during coating growth in pulsed magnetron sputtering discharges. Thin Solid Films **517**(19), 5605–5610 (2009). https://doi.org/10.1016/j.tsf.2009.01.190
15. C. Muratore, J.J. Hu, B. Wang, et al., Continuous ultra-thin MoS_2 films grown by low-temperature physical vapor deposition. Appl. Phys. Lett. **104**, 261604 (2014). https://doi.org/10.1063/1.4885391
16. K. Kang, S. Xie, L. Huang, et al., High-mobility three-atom-thick semiconducting films with wafer-scale homogeneity. Nature **520**, 656 (2015)
17. C. Altavilla, M. Sarno, P. Ciambelli, A novel wet chemistry approach for the synthesis of hybrid 2D free-floating single or multilayer Nanosheets of MS_2@oleylamine (M═Mo, W). Chem. Mater. **23**(17), 3879–3885 (2011). https://doi.org/10.1021/cm200837g
18. H. Schmidt, S. Wang, L. Chu, et al., Transport properties of monolayer MoS_2 grown by chemical vapor deposition. Nano Lett. **14**(4), 1909–1913 (2014). https://doi.org/10.1021/nl4046922
19. Y. Yu, C. Li, Y. Liu, et al., Controlled scalable synthesis of uniform, high-quality monolayer and few-layer MoS_2 films. Sci. Rep. **3**, 1866 (2013)
20. N. Choudhary, J. Park, J.Y. Hwang, et al., Growth of large-scale and thickness-modulated MoS_2 nanosheets. ACS Appl. Mater. Interfaces **6**(23), 21215–21222 (2014). https://doi.org/10.1021/am506198b
21. Y. Lee, X. Zhang, W. Zhang, et al., Synthesis of large-area MoS_2 atomic layers with chemical vapor deposition. Adv. Mater. **24**(17), 2320–2325 (2012). https://doi.org/10.1002/adma.201104798
22. X. Ling, Y. Lee, Y. Lin, et al., Role of the seeding promoter in MoS_2 growth by chemical vapor deposition. Nano Lett. **14**(2), 464–472 (2014). https://doi.org/10.1021/nl4033704
23. E. Lalik, W.I.F. David, P. Barnes, et al., Mechanisms of reduction of MoO_3 to MoO_2 reconciled. J. Phys. Chem. B **105**(38), 9153–9156 (2001). https://doi.org/10.1021/jp011622p
24. D.L. Smith, *Thin Film Deposition: Principles and Practice*, 1st edn. (McGraw-Hill Education, New York, 1995)

25. J. Moser, F. Levy, Growth mechanisms and near-interface structure in relation to orientation of MoS_2 sputtered thin films. J. Mater. Res. **7**(3), 734–740 (1992). https://doi.org/10.1557/JMR.1992.0734
26. G. Seifert, J. Finster, H. Müller, SW Xα calculations and x-ray photoelectron spectra of molybdenum(II) chloride cluster compounds. Chem. Phys. Lett. **75**(2), 373–377 (1980). https://doi.org/10.1016/0009-2614(80)80534-3
27. P.A. Spevack, N.S. McIntyre, Thermal reduction of molybdenum trioxide. J. Phys. Chem. **96**(22), 9029–9035 (1992). https://doi.org/10.1021/j100201a062